

Wave Interpolation Neural Operator: Interpolated Prediction of Electric Fields Across Untrained Wavelengths

Joonhyuk Seo^{1*}, Chanik Kang^{1*}, Dongjin Seo², Haejun Chung^{1†}

¹Department of Artificial Intelligence, Hanyang University, Seoul, South Korea

²Department of Applied Physics, Yale University, USA

{yhy258, chanik, haejun}@hanyang.ac.kr, {dongjin.seo}@yale.edu

Abstract

Designing photonic structures requires electromagnetic simulations, which often require high computational costs. Researchers have developed surrogate solvers for predicting electric fields to alleviate the computational issues. However, existing surrogate solvers are limited to performing inference at fixed simulation conditions and require retraining for different conditions. To address this, we propose Wave Interpolation Neural Operator (WINO), a novel surrogate solver enabling simulation condition interpolation across a continuous spectrum of broadband wavelengths. WINO introduces the Fourier Group Convolution Shuffling operator and a new conditioning method to efficiently predict electric fields from both trained and untrained wavelength data, achieving significant improvements in parameter efficiency and spectral interpolation performance. Our model demonstrates approximately 100 times faster performance than traditional finite-difference frequency-domain simulations. Moreover, compared to the state-of-the-art model, we achieve a 74% reduction in parameters and 80.5% improvements in prediction accuracy for untrained wavelengths, and 13.2% improvements for trained wavelengths.

Introduction

Metalens is at the forefront of next-generation optical technologies. The technology promises to overcome the limitations of high numerical apertures in conventional lenses (Chung and Miller 2020), eliminate chromatic aberration (Seo et al. 2023) and provide unprecedented control over light propagation (Kuznetsov et al. 2024). These advantages offer groundbreaking solutions to previously unsolved challenges in optics. Designing metalenses involves conducting electromagnetic simulations grounded in the partial differential equations (PDEs) called Maxwell's equations. Generally, the simulations numerically solve Maxwell's equations using finite-difference frequency-domain (FDFD) (Hughes et al. 2019, 2018) or finite-difference time-domain (FDTD) (Kunz and Luebbers 1993; Oskooi et al. 2010) solvers. However, the requirement of high computational resources makes large-scale simulations and designs intractable (Kang et al. 2024a). To address this challenge, there is a need for surrogate solvers that operate faster than traditional simulations and provide

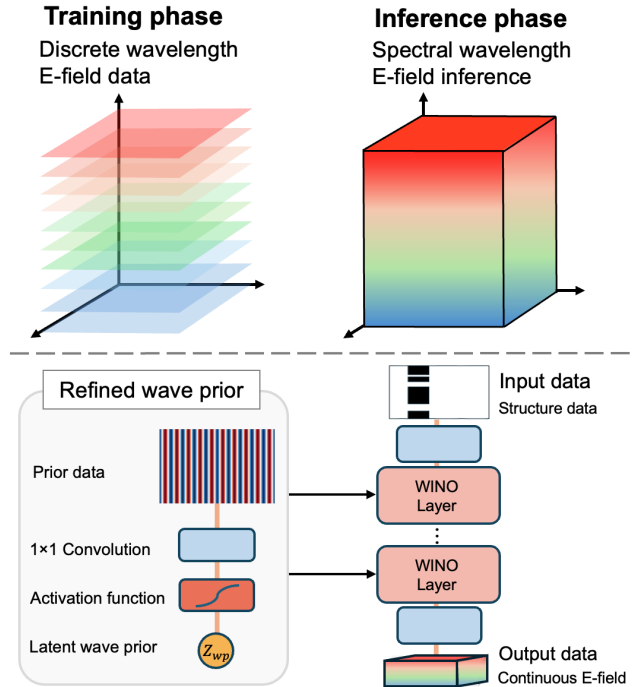


Figure 1: Overall framework of WINO. In the training phase (left section), the model is trained using discrete wavelength electric field data and the refined wave prior of WINO. In the inference phase (right section), the trained model, comprising WINO layers, takes a photonic structure as input data and infers the electric field across the spectral wavelength.

precise results.

Recent studies (Lim and Psaltis 2022; Mao et al. 2024) have focused on developing surrogate solvers that approximate electromagnetic simulations, where the solvers generally use neural networks because of their rapid inference speed. Most previous studies have employed conventional data-driven neural networks to predict plausible results based on a constrained number of design factors (Jiang et al. 2019; Kang et al. 2024b). However, as demonstrated in a prior study (Kovachki et al. 2023), these models frequently fail to guarantee discretization invariance. This poses difficulties in learning PDEs with mesh information that changes according to wave-

*These authors contributed equally.

†Corresponding author.

length or resolution. Several approaches, such as Physics-Informed Neural Networks (PINNs) (Raissi, Perdikaris, and Karniadakis 2019; Lim and Psaltis 2022; Chen et al. 2022), directly integrate physical information into the training process by constructing loss functions derived from physical PDEs. Despite these advances, training neural networks to approximate PDE solutions is computationally intensive, particularly for high-dimensional and nonlinear problems. Furthermore, PINNs typically perform well within the fixed simulation settings in which they are trained. Generating a new dataset and retraining the model to predict outcomes for new simulation parameters are necessary. Recent advances in neural operators (Kovachki et al. 2023; Li et al. 2020; Tran et al. 2021) have focused on achieving discretization invariance while learning the characteristics of PDEs. In particular, Fourier Neural Operator (FNO) has demonstrated excellent performance and efficiency in various applications. However, FNO typically does not have normalization and a bottleneck structure like (Ronneberger, Fischer, and Brox 2015; Vaswani et al. 2017), thereby requiring a novel conditioning method. Consequently, previous works have focused on incorporating condition information into FNOs. For instance, (Gupta and Brandstetter 2022; Mao et al. 2024) embedded condition factors as vectors and modulated weights in the Fourier layers, thereby allowing different weights for varying conditions.

However, this conditioning method struggles to achieve good performance under untrained conditions. One of the most parameter-efficient operators for learning electromagnetic simulations, NeurOLight (Gu et al. 2022), performed using prior data constructed from wave equations that directly encode light propagation characteristics. This approach enables interpolation across parameters such as grid steps and wavelengths. Despite these strengths, NeurOLight's dependence on minor grid step variations and conditioning through simple concatenation with input data restricts its learning and inference capabilities to a limited range of wavelengths and grid steps.

To address this problem, we propose a parameter-efficient surrogate solver named Wave Interpolation Neural Operator (WINO). For the first time, WINO enables the interpolation of simulation parameters by training with discrete wavelength simulation data, allowing it to infer across a continuous spectrum of broadband wavelengths. The main contributions of our study are as follows:

1. To the best of our knowledge, our work presents the first broadband electromagnetic surrogate solver.
2. WINO is approximately 100 times faster than FDFD simulation.
3. Parameter efficiency improves by approximately 74% over the previous state-of-the-art (SOTA) model.
4. Performance improvements: 81% enhancement for untrained wavelengths and 10% enhancement for trained wavelengths compared to the SOTA.

Related Work

Neural Network-Based Approximations

Light is an electromagnetic wave, and its behavior is governed by PDEs known as Maxwell's equations. Maxwell's

equations describe the electromagnetic behavior of light such as the mutual induction of electric and magnetic fields, the propagation of light waves, and the interaction of light with matter. Previous efforts in electromagnetic field prediction have focused on training neural networks to approximate field values. Data-driven neural network research (Jiang, Chen, and Fan 2021; Trivedi et al. 2019; An et al. 2020) attempted to learn and predict Maxwell's equations using simulated field data. However, these approaches often struggled to accurately capture the physical characteristics of Maxwell's equations. To address this issue, Physics-Informed Neural Networks (PINNs) were employed in Physics-Augmented Deep Learning research (Chen et al. 2022). This method combined data loss and Maxwell loss as the total loss, integrating Maxwell's equations into the field prediction process for given structures. While this approach improved prediction speed compared to traditional FDFD solvers, it still had significant limitations. Specifically, it required datasets for each individual wavelength and could only predict fields for the trained wavelengths. Additionally, the field predictions were confined to small and simple photonic structures.

Advancements in Operator Learning

Previous research using data-driven approaches has struggled to accurately learn and infer the characteristics of Maxwell's equations. As a result, researchers have begun exploring neural network-based operators designed to model and predict complex physical systems (Azizzadenesheli et al. 2024; Li et al. 2020). Recent advancements in the field of Operator Learning offer promising solutions that effectively learn PDE characteristics while preserving discretization invariance. The FNO proposed by (Li et al. 2020) presents a deep learning architecture designed to learn mappings between infinite-dimensional function spaces. This approach significantly enhances the efficiency and accuracy of solving PDEs. The FNO achieves resolution invariance and supports zero-shot super-resolution, establishing it as a pioneering method in operator learning. After FNO has been published, the Factorized-FNO (Tran et al. 2021), named F-FNO, improves the performance of the original FNO by using separable spectral layers and enhanced residual connections, significantly reducing errors in various PDE problems. In electromagnetic field prediction, the state-of-the-art model NeurOLight (Gu et al. 2022) leverages the FNO. (Gu et al. 2022) encodes wave prior by combining wavelength information and material permittivity, effectively learning the PDEs of Maxwell's equations. The model has demonstrated superior parameter efficiency and higher accuracy compared to previous studies. However, it still has limitations as it predicts fields for a limited narrow range of wavelengths and grid steps, making it less suitable for broadband wavelength applications.

Methodology

Comprehending Optical Field Simulation

To collect training and validation datasets, we employ the FDFD method which is one of the numerical methods used to solve Maxwell's equations.

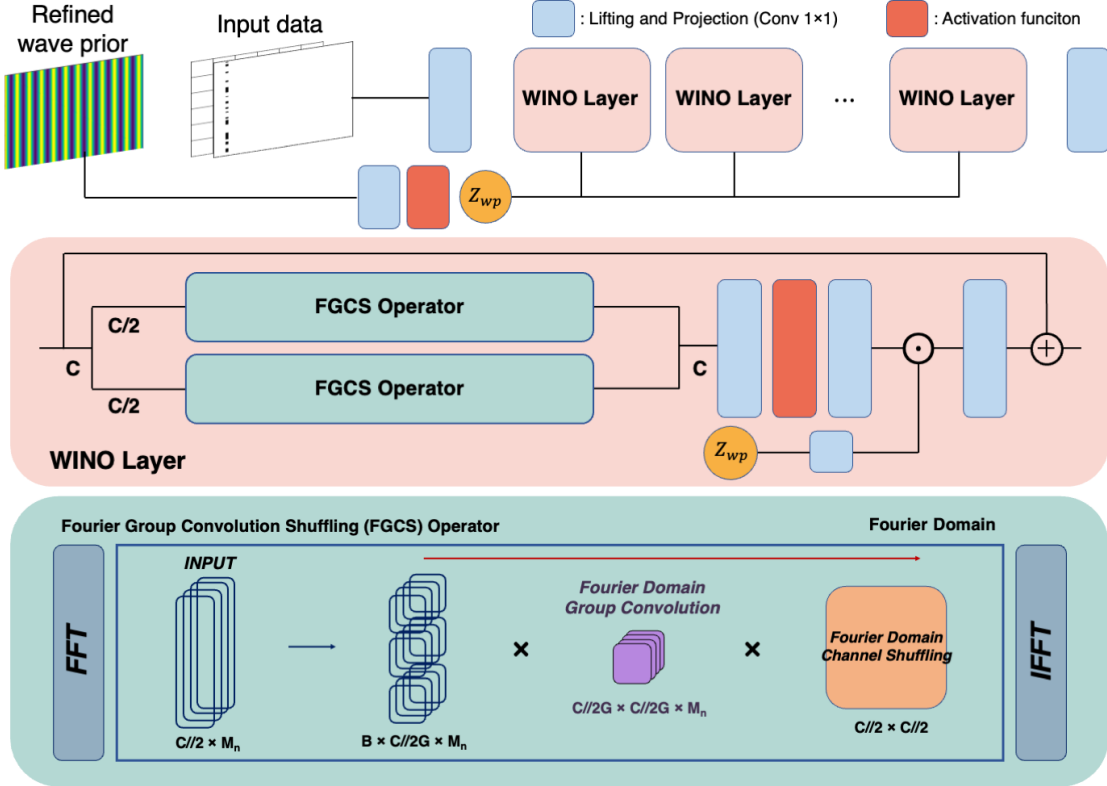


Figure 2: Schematic illustration of (top) Wave Interpolation Neural Operator (WINO) including (middle) WINO layer and (bottom) Fourier Group Convolution Shuffling (FGCS) operator.

The FDFD method discretizes the spatial domain into coordinates and solves electromagnetic fields in the frequency domain, making it particularly effective for steady-state analysis. This method is especially effective for generating field data for single frequencies as light passes through the metalens. Resonances can occur in subwavelength photonic structures and significantly affect their performance. However, predicting the resonance of electric fields in subwavelength structures becomes challenging when the wavelength changes due to the nonlinearity of resonance (Dorodnyy, Smajic, and Leuthold 2023; Nieto-Vesperinas 2020). Therefore, surrogate solvers trained on specific wavelengths struggle to predict fields for different wavelengths, even when applied to the same structure. For a detailed explanation of the nonlinearity of resonance, refer to the Appendix section titled “Nonlinearity of Subwavelength Photonic Structure Resonance.”

Wave Interpolation Neural Operator

We propose Wave Interpolation Neural Operator (WINO), which enables the interpolated prediction of unseen wavelengths from simulation observations of discrete wavelengths (Figure 2). WINO comprises two main components: (1) the Fourier Group Convolution Shuffling (FGCS) operator that is designed to be highly parameter-efficient while maintaining performance, and (2) a novel conditioning method that enables the seamless interpolation of data conditions.

Let $\Omega \subset \mathbb{R}^d$, $\mathcal{A} = \mathcal{A}(\Omega; \varepsilon^{d_a})$ where $\varepsilon = \{\epsilon_{\text{air}}, \epsilon_{\text{material}}\}$, and $\mathcal{U} = \mathcal{U}(\Omega; \mathbb{C}^{d_u})$ be a bounded open set of the underlying

domain, infinite-dimensional spaces of the relative permittivity and field of the simulation. ϵ_{air} and $\epsilon_{\text{material}}$ represent the relative permittivity values of air and material. Additionally, we assume that $\mathcal{W} \subset \mathbb{R}_{\geq 0}$ is the broadband range, such as the visible light spectrum, and $\tilde{\mathcal{W}} \subset \mathcal{W}$ is a discrete collection of wavelengths evenly distributed at a specific interval from \mathcal{W} . Our model G_θ learns an ideal electromagnetic simulator $G^\dagger : \mathcal{A} \rightarrow \mathcal{U}$ for continuous wavelengths \mathcal{W} by mapping between infinite-dimensional function spaces using a finite set of Maxwell PDE input-output pairs $\{(w_j, a_j), u_j\}_{j=1}^N$, where $w \in \tilde{\mathcal{W}}$.

Similar to a prior work (Kovachki et al. 2023), WINO has an iterative process to map between infinite-dimensional function spaces.

$$u = \mathcal{G}_\theta(a) = (\mathcal{Q} \circ \mathcal{L}^{(L)} \circ \dots \circ \mathcal{L}^{(1)} \circ \mathcal{P})(a)$$

where $\mathcal{L}^{(l)}$ is a l -th operator layer, L indicates the number of layers, and \mathcal{P}, \mathcal{Q} are lifting and projection operators, respectively.

We define the WINO layers $\mathcal{L}^{(l)}$ as follows:

$$\mathcal{L}^{(l)}(z^{(l)}) = z^{(l)} + W_2^{(l)} \sigma(W_1^{(l)} \tilde{\mathcal{K}}^{(l)}(z^{(l)}) + b_1^{(l)}) + b_2^{(l)}$$

We employ a residual connection after two linear transformations with an activation function to enhance the capacity of our model, like (Vaswani et al. 2017; Tran et al. 2021). In addition, we use 1×1 convolution layers instead of 3×3 convolution layers to ensure discretization invariance unlike a previous study (Gu et al. 2022).

Kernel Integral Operator $\tilde{\mathcal{K}}$ of WINO The kernel integral operator in the original FNO is defined as follows:

$$\mathcal{K}^{(l)} = \mathcal{F}^{-1}(R^{(l)} \cdot \mathcal{F}), \quad R \in \mathbb{C}^{M_v \times M_h \times C \times C}$$

where \mathcal{F} is a Fourier transformation, M_v , M_h , and C denote the number of frequency modes of vertical and horizontal components and the number of channels, respectively. Thus, the number of parameters in a 2D problem is $C^2 M_v M_h$. This leads to a significantly high parameter complexity. Thus, as illustrated in Figure 2 (middle), we construct the cross-shaped block (Gu et al. 2022) to achieve superior parameter efficiency. We split the inputs into two chunks $z^{(l)} = [z_h^{(l)}, z_v^{(l)}]$ along the channel axis and factorize the Fourier transforms over the horizontal and vertical dimensions $\tilde{\mathcal{K}}^{(l)}(z^{(l)}) = [\mathcal{K}_h^{(l)}(z_h^{(l)}), \mathcal{K}_v^{(l)}(z_v^{(l)})]$. Therefore, the weights $R_h^{(l)} \in \mathbb{C}^{M_h \times \frac{1}{2}C \times \frac{1}{2}C}$ and $R_v^{(l)} \in \mathbb{C}^{M_v \times \frac{1}{2}C \times \frac{1}{2}C}$ of both two blocks have $\frac{C^2}{4}(M_h + M_v)$ parameters, fewer than the $C^2 M_h M_v$ parameters in the kernel integral operator of an FNO.

Furthermore, we propose an efficient Fourier Group Convolution Shuffling (FGCS) operator that is extremely parameter-efficient while maintaining high performance, as shown in Figure 2 (middle and bottom). We group the input in the Fourier domain along the channel dimension using the group parameter G , as inspired by (Xie et al. 2017; Guibas et al. 2021; Kim, Park, and Shin 2024). Let the horizontal and vertical components be represented by $\mathcal{F}(z_h^{(l)}) \in \mathbb{C}^{H \times M_h \times \frac{1}{2}C}$ and $\mathcal{F}(z_v^{(l)}) \in \mathbb{C}^{M_v \times W \times \frac{1}{2}C}$, respectively. By introducing a group parameter G , horizontal component becomes $\mathcal{F}'(z_h^{(l)}) \in \mathbb{C}^{H \times M_h \times G \times \frac{1}{2G}C}$, and the vertical component is transformed into $\mathcal{F}'(z_v^{(l)}) \in \mathbb{C}^{M_v \times W \times G \times \frac{1}{2G}C}$. Different weights are assigned to each group, denoted as $R^{(l)} \in \mathbb{C}^{M \times G \times \frac{1}{2G}C \times \frac{1}{2G}C}$. This grouping in the Fourier domain allows for more efficient parameterization with a parameter complexity of $C^2 M/G$. To achieve even higher parameter efficiency, we share weights across the divided groups by defining the horizontal and vertical weights as $R_h^{(l)} \in \mathbb{C}^{M_h \times \frac{1}{2G}C \times \frac{1}{2G}C}$ and $R_v^{(l)} \in \mathbb{C}^{M_v \times \frac{1}{2G}C \times \frac{1}{2G}C}$, respectively. Consequently, we construct a kernel integral operator with a parameter complexity of $C^2 M/G^2$. However, the weight-sharing scheme in the group convolution leads to a significant information loss compared to independent weight methods, resulting in a drastic performance decline. Thus, we further perform channel shuffling in the Fourier domain, which can be functioned through simple matrix multiplication along the channel dimension with $W_{\text{ch}}^{(l)} \in \mathbb{C}^{1 \times 1 \times C \times C}$. The channel shuffling scheme can compensate for the lost information by weight-sharing group convolution, thereby preserving performance while achieving exceptional parameter efficiency.

Novel Conditioning Method for Interpolating Untrained Wavelengths’ Simulations The changes in the field wave patterns with varying wavelengths, along with resonance and diffraction phenomena during wave-material interactions, are highly nonlinear. This nonlinearity presents challenges in predicting simulation fields for unseen wavelengths during

training. Therefore, interpolation for broadband spectrum parameter space requires condition information that accurately reflects the wave characteristics and a conditioning method that appropriately injects the condition.

First, we propose a conditioning method for interpolation in the parameter space of the broadband spectrum, as shown in Figure 2 (top and middle). We assume that the condition data have high spatial structure similarity with fields and accurately reflect the features of the wave patterns. Under these assumptions, preserving the spatial structure of the condition information when constructing high-dimensional embeddings is necessary to reflect the field changes according to continuous wavelengths accurately. Thus, we create a common embedding, which is then injected into all layers, using a 1×1 convolutional layer with a nonlinear activation function. Then, each layer adaptively transforms the embedding using an additional 1×1 convolutional layer. We highlight that employing only channel-wise operations guarantees the preservation of the spatial structure of conditional information, which is substantially similar to the field. The final conditional embeddings created in each layer are element-wisely multiplied with the output of the feed-forward network before the residual connection in each layer. By injecting the condition into all kernel operators through element-wise multiplication, we strongly regularize the spatial and structural information of the field patterns according to the varying wavelengths while the satisfying discretization invariance.

Next, we construct condition information that accurately reflects the wave characteristics by employing a wave prior (Gu et al. 2022). The wave prior is an artificial wave pattern derived from the solution of the wave equation and is expressed as $\mathcal{W}_x = e^{j \frac{2\pi\sqrt{\epsilon_r}}{\lambda} x \mathbf{1}^T \Delta l_x}$ and $\mathcal{W}_z = e^{j \frac{2\pi\sqrt{\epsilon_r}}{\lambda} z \mathbf{1}^T \Delta l_z}$. Here, $\epsilon_r \in \mathbb{C}^{H \times W}$ represents the relative permittivity of the structures at each coordinate, λ is the wavelength, Δl_x and Δl_z are the simulation’s step length, and x and z are the coordinates. Because the wave prior emulates the solution of the wave equation, it is substantially similar to the wave patterns of the field generated by the simulator, which result from light propagation according to wavelengths, achieving the precluded assumption. However, the wave prior considers only the structures’ permittivity values without accounting for the diffraction phenomena, because it is defined by simultaneously reflecting coordinates. The wave prior exhibits sharp and physically implausible features in the regions where the permittivity values change (Figure A4 (top left and right)). Moreover, our conditioning method utilizes shallow 1×1 convolutional layers, which have no receptive field, to preserve the spatial structure of the condition. This feature makes it difficult for learned wave prior data to account for highly nonlinear phenomena, such as diffraction, which result from interactions between structures and waves. The use of 1×1 convolutional layers for processing wave prior causes physically implausible features to remain in the output of the WINO layer. In addition, since the simulation’s permittivity information is already provided as input data, including it in the wave prior is redundant. Hence, we propose a refined wave prior that excludes the ϵ_r term, defined

as $\mathcal{W}_x = e^{j\frac{2\pi}{\lambda}x\mathbf{1}^T\Delta l_x}$ and $\mathcal{W}_z = e^{j\frac{2\pi}{\lambda}\mathbf{1}z^T\Delta l_z}$ (Figure A4 (bottom left)). The refined condition information aims to provide a more physically plausible representation of light behavior in free space. As the influence of simulation parameters like higher relative permittivity increases, the nonlinear optics effects become more pronounced, and the precluded assumption weakens. However, we find that our method still works reasonably well even in these cases. For a detailed experiments, refer to the Appendix section titled "Additional Experiments for the Weakened Precluded Assumption."

Experiments

Experiment Setup

FDFD Simulation Setup In our study, we utilize Ceviche (Hughes et al. 2019), an open-source FDFD simulation tool, to generate electromagnetic field data for photonic structures. Specifically, we analyze the field of a metlens structure, simulating only half of the cylindrical symmetry lens to reduce computation time. We implement the FDFD simulation with a grid-based approach at a spatial resolution of 40 points per μm . The simulation domain measures $5.2\ \mu\text{m} \times 6.85\ \mu\text{m}$, excluding a $1\text{-}\mu\text{m}$ thick perfectly matched layer (PML) at the boundaries. We use SiO_2 , a material commonly employed in the design of metlenses (Park et al. 2019). As demonstrated in Figure 3 (left), we randomly place either SiO_2 or air within the minimum design grid size, a width of 75nm , in the design area. This simulation setup generates data for the E and H fields when visible light passes through the structure.

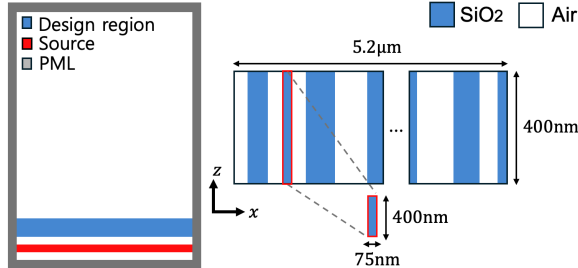


Figure 3: FDFD simulation setup overview. (left) The entire simulation space includes the metlens structure. The blue region represents the design region of the lens, red line represents the visible light source, and the gray region represents the PML used to minimize reflections. (right) The design region of the metlens, shown as the blue area in (left).

Datasets We aim to predict the E-field for all wavelengths from discrete data in the 400-700nm (visible light) range. To achieve this, we generate field data for discrete wavelengths as our dataset. Different lens structures are randomly placed in the design region for each data, and the field data resulting from FDFD simulations, along with the permittivity(ε) of the materials, wavelength(λ), and structural information, are used as pairs for training. Specifically, the training set consists of 12,000 data sampled randomly at 20nm intervals within the 400-700nm wavelength range. As mentioned above, our goal is to achieve seamless field prediction across the broadband

wavelength. Therefore, to use unseen data for testing, we use 6,020 data each for the test and validation sets, composed of 20 data for each wavelength, sampled at 1nm intervals between 400 and 700nm.

Training Objective and Evaluation Metric Fields typically exhibit different statistics despite the fixed source power. We employ the normalized mean squared error (N-MSE) objective, $L(G_\theta(a), G^\dagger(a)) = (\|G_\theta(a) - G^\dagger(a)\|_2^2 / \|G^\dagger(a)\|_2^2)$, to distribute the optimization effort evenly across several field data. We also use N-MSE for evaluation.

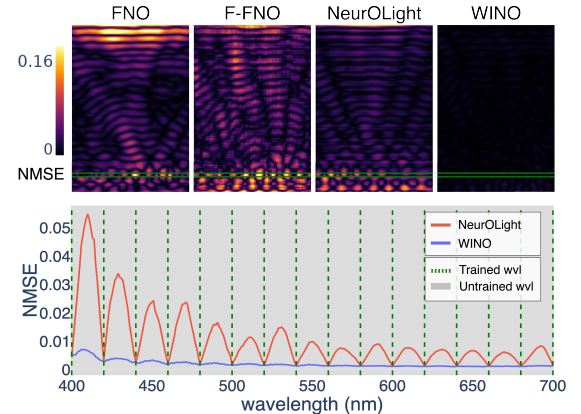


Figure 4: Field interpolation comparisons. (top) Comparison of model errors at 410nm, the unobserved wavelength with the highest error. Darker colors indicate lower errors. Other models show generally high errors in both the design region (green) and the overall area, our model. Nevertheless, WINO demonstrates near-zero errors across the entire area, including the design region. (bottom) Comparison of entire simulation region errors in the 400-700nm wavelength range. Our model outperforms the previous SOTA model, NeurOLight, in field prediction performance across the entire wavelength range.

Results

In the following, we compare the interpolation performance for unobserved wavelengths of Unet (Ho, Jain, and Abbeel 2020; Gupta and Brandstetter 2022), FNO (Li et al. 2020), and F-FNO (Tran et al. 2021), commonly used in a surrogate solver study. Moreover, we evaluate WINO against NeurOLight (Gu et al. 2022), the state-of-the-art model for single wavelength field prediction in electromagnetic simulation. Detailed information on model architectures is in the Appendix section titled "Detailed model architectures."

In EM simulation, while predicting the entire E-field is important, accurately predicting the E-field within the design region is even more crucial. For studies involving surrogate solvers to predict E-fields and subsequently optimize designs, error-free predictions in the design region are essential for designing high-performance photonic devices.

However, existing models struggle with the nonlinear resonances observed in design regions. These resonances can vary with different source wavelengths, even for the same structure, leading to significant errors in interpolation.

Model	Param (M)	Test loss		Design region test loss	
		Untrained	Trained	Untrained	Trained
Unet (Ho, Jain, and Abbeel 2020)	11.5999	0.003332	0.001732	0.00619	0.003775
FNO (Li et al. 2020)	3.2868	0.0133	0.007719	0.028339	0.025067
F-FNO (Tran et al. 2021)	1.887	0.03309	0.02204	0.043035	0.037091
NeurOLight (Gu et al. 2022)	1.65	0.01073	0.001973	0.019503	0.004526
WINO	0.426	0.002035	0.001774	0.003812	0.003929

Table 1: Comparisons of field prediction and interpolation. Untrained represents the loss when predicting fields using unobserved wavelength data, which is the loss for the wavelength interpolation.

As shown in Figure 4 (top), all models except our WINO exhibit significant errors in the design region. Such resonance patterns can occur in the metalens used in our experiments and other photonic structures designed at the sub-wavelength scale. Therefore, our model can accurately predict resonance patterns during wavelength interpolation in the design region, making it broadly applicable. Furthermore, we aimed to improve the overall error compared to the SOTA and significantly reduce the error in the design region.

Our wave interpolation results achieved SOTA performance in both test loss across the entire region and loss in the design region, compared to existing models (Li et al. 2020; Tran et al. 2021; Gu et al. 2022) as shown in Figure 4 (bottom), Table 1 and Figure A1. Specifically, in the design region, which is represented in Table 1 and Figure A2, our model showed an impressive 80.5% improvement over the previous SOTA model, NeurOLight, for untrained wavelengths and an improvement of 13.2% for trained wavelengths. Moreover, we aimed to drastically reduce the number of parameters, achieving a SOTA model with only 0.426 million parameters, a 74.18% reduction compared to NeurOLight and a 96.33% reduction compared to Unet. Hence, our model demonstrates performance on par with the existing SOTA models for trained wavelengths while achieving the highest level of performance in interpolation and model parameter reduction in the current research.

Ablation Study

Hyperparameters of FGCS Operator We assess the validity of the hyperparameters (groups and channels) and design choices (weight sharing and channel shuffling) of the proposed FGCS operator by conducting an extensive ablation study, as shown in Table 2. We increase the number of groups in proportion to the growth of channels to consider a consistent number of parameters in all cases. Row 9 presents the FGCS operator used in our model. Rows 1-3, which do not utilize weight sharing and channel shuffling in the Fourier domain, follow the same operational form as described in a previous study (Kim, Park, and Shin 2024). When only weight sharing is employed (rows 4-5), the prediction of fields for both unobserved and observed wavelengths during the training phase demonstrates worse performance compared to that in a previous study (Kim, Park, and Shin 2024) due to information loss in a lower channel due to a substantially small number of parameters. However, as the number of groups and channels increases, the performance becomes competitive. Notably, the performance in predict-

ing the fields for unobserved wavelengths during training is better. Thus, the weight-sharing scheme significantly aids in generalizing the unobserved spectral parameters.

Weight sharing	Channel shuffling	Groups	Channels	Params	Test loss	
					Untrained	Trained
		1	32	0.423	0.00413	0.00361
		2	48	0.562	0.00278	0.00193
		4	64	0.654	0.00251	0.00165
✓		2	48	0.372	0.00398	0.00342
✓		4	64	0.401	0.00234	0.00199
	✓	2	48	0.576	0.0033	0.00276
	✓	4	64	0.679	0.00211	0.00153
✓	✓	2	48	0.386	0.00366	0.00302
✓	✓	4	64	0.426	0.00204	0.00177
		8	128	1.898	0.00162	0.00092
✓		8	128	1.306	0.00123	0.00091
	✓	8	128	1.996	0.00145	0.00081
✓	✓	8	128	1.405	0.00105	0.00081

Table 2: Ablation of design components of proposed FGCS operator. The ✓ indicates the use of the design components.

In addition, comparing the previous method (Kim, Park, and Shin 2024) (rows 2-3) with the case where only channel shuffling is utilized (rows 6-7), the field prediction performance for both the untrained and trained wavelengths is better. This suggests that employing the channel shuffling method with the grouping method significantly improves the overall performance. Following the design configuration of the FGCS operator (rows 8-9), we can construct a parameter-efficient model that achieves an overall performance improvement as the number of groups and channels is heightened. While the FGCS operator shows slightly lower prediction performance for untrained wavelengths than when only a channel shuffling scheme is employed, it demonstrates superior performance for trained wavelengths. Therefore, the proposed FGCS operator contributes to improving interpolation performance for unseen broadband spectrum parameters during training. Rows 10-13 present varying performances when increasing the model width. The performance improvement of the FGCS operator becomes increasingly significant with the addition of more channels. In particular, there is a substantial improvement when the number of groups and channels increases to 8 and 128, respectively. We believe that excessively sparse constructions of weights tensor and infor-

mation compensating with channel shuffling may improve the generalization capacity of large models.

Conditioning Methods We conduct a comparative analysis of our proposed method and two other conditioning methods to evaluate our conditioning method’s efficacy.

Conditioning method	Params	Test loss	
		Untrained	Trained
Spectral parameter conditioning	1.086	0.13761	0.002577
Concatenating wave prior	0.326	0.002821	0.002022
Our conditioning method	0.426	0.002035	0.001774

Table 3: Ablation study of several conditioning methods.

Table 3 shows the results of the ablation study conducted on WINO. As in the previous experiments, The terms “untrained” and “trained” represent the setups in which fields are predicted using untrained and trained wavelength data, respectively. The conditioning methods used for comparison are spectral parameter conditioning (Gupta and Brandstetter 2022; Mao et al. 2024) and the concatenating wave prior (Gu et al. 2022). The spectral parameter conditioning method transforms the scalar wavelength into a vector via sinusoidal embedding (Vaswani et al. 2017). It then employs a two-layer feed-forward network to project the embeddings onto a higher-dimensional space of $4 \times$ hidden channels. The embeddings are mapped to the Fourier space using the module named FreqLinear module described in (Gupta and Brandstetter 2022). Finally, the embeddings in the Fourier space are mode-wise multiplied with the input of the Fourier integral kernel to perform parameter conditioning in the spectral domain. The concatenating wave prior injects the condition information by simply concatenating the given refined wave prior to the input data. Although the spectral parameter conditioning method effectively predicts the fields of wavelengths observed during training, it fails to perform interpolation in the parameter space of the broadband spectrum. Thus, the spectral parameter conditioning method is incapable of learning the patterns of fields with continuously varying wavelengths. Our conditioning method thoroughly outperforms the concatenating wave prior conditioning method in both the trained and untrained wavelength cases, achieving a 12.3% improvement in trained wavelengths and a 27.9% improvement in untrained wavelengths. Consequently, the proposed method is effective for injecting conditions that are substantially similar to the fields in terms of the spatial and structural features. Furthermore, we conducted an additional comparative analysis between our conditioning method and other methods using various models. For a detailed explanation of the more ablation studies, refer to the Appendix section titled “Additional Ablation Studies for Conditioning Methods.”

Permittivity in the Wave Prior As shown in Table 4, we demonstrate performance enhancement resulting from the exclusion of the ϵ_r term from the wave prior through an ablation study. To identify the reason for the improvement, we investigate the latent wave prior and the output of the last

ϵ_r term	Test loss	
	Untrained	Trained
✓	0.002372	0.002148
✗	0.002035	0.001774

Table 4: Ablation study for ϵ_r term in wave prior.

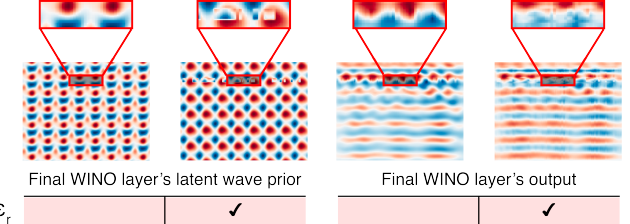


Figure 5: Visualization of the features of condition information and outputs from the final WINO layers for a specific part of the entire region for 400nm wavelength data. (left) The latent wave prior in the final WINO layer, excluding and including the ϵ_r term. (right) The output of the final WINO layer without and with considering the ϵ_r term. The magnified sections are part of the region where structures exist.

WINO layer. Figure 5 (left) shows the latent wave prior before element-wise multiplication in the last WINO layer. Sharp features emerge in regions with structures when the wave prior reflects the ϵ_r term because our conditioning method utilizes shallow 1×1 convolutional layers to ensure the discretization invariance property and maintain the spatial structure of the refined wave prior. Figures 5 (right) show the outputs of the final WINO layer. The result in Figure 5 (right), where the ϵ_r term is included in the wave prior, has bizarre features present throughout the entire region compared to when the ϵ_r term is not included. Therefore, we conclude that the ϵ_r term in the wave prior introduces unintended bias.

Conclusion

In this study, we introduce the Wave Interpolation Neural Operator (WINO), a novel surrogate solver designed to address the limitations of existing models in predicting electric fields across a continuous spectrum of wavelengths. By leveraging Fourier Group Convolution Shuffling (FGCS) and a new conditioning method, WINO significantly improves parameter efficiency and interpolation performance. Our experimental results demonstrate that WINO achieves state-of-the-art performance in both test loss and design region test loss compared to existing models such as FNO, F-FNO, and the previous SOTA, NeurOLight. Specifically, WINO exhibits an 80.5% improvement over NeurOLight for unobserved wavelengths and a 13.2% enhancement for trained wavelengths. Additionally, the number of parameters is reduced by 74.18% compared to NeurOLight and 96.33% compared to Unet. Furthermore, WINO accurately predicts the nonlinear resonance patterns in photonic structures.

This capability and SOTA performance position WINO as a powerful tool, paving the way for broadband photonic applications and enabling the design of highly complex photonic structures with a surrogate solver.

References

An, S.; Zheng, B.; Shalaginov, M. Y.; Tang, H.; Li, H.; Zhou, L.; Ding, J.; Agarwal, A. M.; Rivero-Baleine, C.; Kang, M.; et al. 2020. Deep learning modeling approach for metasurfaces with high degrees of freedom. *Optics Express*, 28(21): 31932–31942.

Azizzadenesheli, K.; Kovachki, N.; Li, Z.; Liu-Schiaffini, M.; Kossaifi, J.; and Anandkumar, A. 2024. Neural operators for accelerating scientific simulations and design. *Nature Reviews Physics*, 1–9.

Chen, M.; Lupoiu, R.; Mao, C.; Huang, D.-H.; Jiang, J.; Lalanne, P.; and Fan, J. A. 2022. High speed simulation and freeform optimization of nanophotonic devices with physics-augmented deep learning. *ACS Photonics*, 9(9): 3110–3123.

Chung, H.; and Miller, O. D. 2020. High-NA achromatic metalenses by inverse design. *Optics Express*, 28(5): 6945–6965.

Dorodnyy, A.; Smajic, J.; and Leuthold, J. 2023. Mie scattering for photonic devices. *Laser & Photonics Reviews*, 17(9): 2300055.

Gu, J.; Gao, Z.; Feng, C.; Zhu, H.; Chen, R.; Boning, D.; and Pan, D. 2022. Neurolight: A physics-agnostic neural operator enabling parametric photonic device simulation. *Advances in Neural Information Processing Systems*, 35: 14623–14636.

Guibas, J.; Mardani, M.; Li, Z.; Tao, A.; Anandkumar, A.; and Catanzaro, B. 2021. Adaptive fourier neural operators: Efficient token mixers for transformers. *arXiv preprint arXiv:2111.13587*.

Gupta, J. K.; and Brandstetter, J. 2022. Towards multi-spatiotemporal-scale generalized pde modeling. *arXiv preprint arXiv:2209.15616*.

Ho, J.; Jain, A.; and Abbeel, P. 2020. Denoising diffusion probabilistic models. *Advances in neural information processing systems*, 33: 6840–6851.

Hughes, T. W.; Minkov, M.; Williamson, I. A.; and Fan, S. 2018. Adjoint method and inverse design for nonlinear nanophotonic devices. *ACS Photonics*, 5(12): 4781–4787.

Hughes, T. W.; Williamson, I. A.; Minkov, M.; and Fan, S. 2019. Forward-mode differentiation of Maxwell’s equations. *ACS Photonics*, 6(11): 3010–3016.

Jiang, J.; Chen, M.; and Fan, J. A. 2021. Deep neural networks for the evaluation and design of photonic devices. *Nature Reviews Materials*, 6(8): 679–700.

Jiang, J.; Sell, D.; Hoyer, S.; Hickey, J.; Yang, J.; and Fan, J. A. 2019. Free-form diffractive metagrating design based on generative adversarial networks. *ACS nano*, 13(8): 8872–8878.

Kang, C.; Park, C.; Lee, M.; Kang, J.; Jang, M. S.; and Chung, H. 2024a. Large-scale photonic inverse design: computational challenges and breakthroughs. *Nanophotonics*.

Kang, C.; Seo, D.; Boriskina, S. V.; and Chung, H. 2024b. Adjoint method in machine learning: a pathway to efficient inverse design of photonic devices. *Materials & Design*, 239: 112737.

Kim, M.; Park, J.; and Shin, J. 2024. Efficient Fourier Neural Operators by Group Convolution and Channel Shuffling. In *ICLR 2024 Workshop on AI4DifferentialEquations In Science*.

Kovachki, N.; Li, Z.; Liu, B.; Azizzadenesheli, K.; Bhattacharya, K.; Stuart, A.; and Anandkumar, A. 2023. Neural operator: Learning maps between function spaces with applications to pdes. *Journal of Machine Learning Research*, 24(89): 1–97.

Kunz, K. S.; and Luebbers, R. J. 1993. *The finite difference time domain method for electromagnetics*. CRC press.

Kuznetsov, A. I.; Brongersma, M. L.; Yao, J.; Chen, M. K.; Levy, U.; Tsai, D. P.; Zheludev, N. I.; Faraon, A.; Arbabi, A.; Yu, N.; et al. 2024. Roadmap for optical metasurfaces. *ACS photonics*, 11(3): 816–865.

Li, Z.; Kovachki, N.; Azizzadenesheli, K.; Liu, B.; Bhattacharya, K.; Stuart, A.; and Anandkumar, A. 2020. Fourier neural operator for parametric partial differential equations. *arXiv preprint arXiv:2010.08895*.

Lim, J.; and Psaltis, D. 2022. MaxwellNet: Physics-driven deep neural network training based on Maxwell’s equations. *ApL Photonics*, 7(1).

Mao, C.; Lupoiu, R.; Dai, T.; Chen, M.; and Fan, J. A. 2024. Towards General Neural Surrogate Solvers with Specialized Neural Accelerators. *arXiv preprint arXiv:2405.02351*.

Nieto-Vesperinas, M. 2020. Fundamentals of Mie scattering. In *Dielectric Metamaterials*, 39–72. Elsevier.

Oskooi, A. F.; Roundy, D.; Ibanescu, M.; Bermel, P.; Joannopoulos, J. D.; and Johnson, S. G. 2010. MEEP: A flexible free-software package for electromagnetic simulations by the FDTD method. *Computer Physics Communications*, 181(3): 687–702.

Park, J.-S.; Zhang, S.; She, A.; Chen, W. T.; Lin, P.; Yousef, K. M.; Cheng, J.-X.; and Capasso, F. 2019. All-glass, large metalens at visible wavelength using deep-ultraviolet projection lithography. *Nano letters*, 19(12): 8673–8682.

Raissi, M.; Perdikaris, P.; and Karniadakis, G. E. 2019. Physics-informed neural networks: A deep learning framework for solving forward and inverse problems involving nonlinear partial differential equations. *Journal of Computational physics*, 378: 686–707.

Ronneberger, O.; Fischer, P.; and Brox, T. 2015. U-net: Convolutional networks for biomedical image segmentation. In *Medical image computing and computer-assisted intervention–MICCAI 2015: 18th international conference, Munich, Germany, October 5–9, 2015, proceedings, part III* 18, 234–241. Springer.

Seo, J.; Jo, J.; Kim, J.; Kang, J.; Kang, C.; Moon, S.; Lee, E.; Hong, J.; Rho, J.; and Chung, H. 2023. Deep-learning-driven end-to-end metalens imaging. *arXiv preprint arXiv:2312.02669*.

Tran, A.; Mathews, A.; Xie, L.; and Ong, C. S. 2021. Factorized fourier neural operators. *arXiv preprint arXiv:2111.13802*.

Trivedi, R.; Su, L.; Lu, J.; Schubert, M. F.; and Vuckovic, J. 2019. Data-driven acceleration of photonic simulations. *Scientific reports*, 9(1): 19728.

Vaswani, A.; Shazeer, N.; Parmar, N.; Uszkoreit, J.; Jones, L.; Gomez, A. N.; Kaiser, Ł.; and Polosukhin, I. 2017. Attention is all you need. *Advances in neural information processing systems*, 30.

Xie, S.; Girshick, R.; Dollár, P.; Tu, Z.; and He, K. 2017. Aggregated residual transformations for deep neural networks. In *Proceedings of the IEEE conference on computer vision and pattern recognition*, 1492–1500.

Appendix: Wave Interpolation Neural Operator

Joonhyuk Seo^{1*}, Chanik Kang^{1*}, Dongjin Seo², Haejun Chung^{1†}

¹Department of Artificial Intelligence, Hanyang University, Seoul, South Korea

²Department of Artificial Intelligence, Hanyang University, Seoul, Republic of Korea
 {yhy258, chanik, haejun}@hanyang.ac.kr, {dongjin.seo}@yale.edu

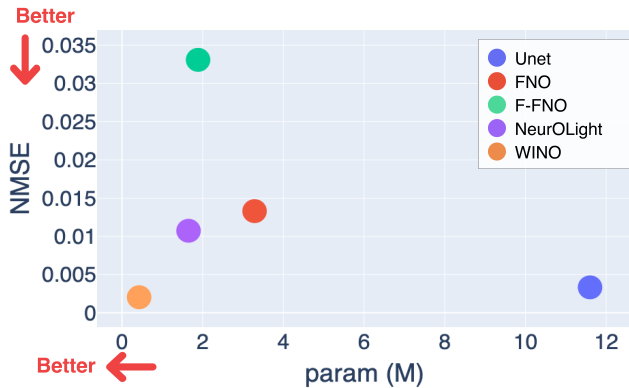


Figure A1: Comparison of WINO with various surrogate solvers in terms of the number of parameters and prediction performance for untrained wavelengths.

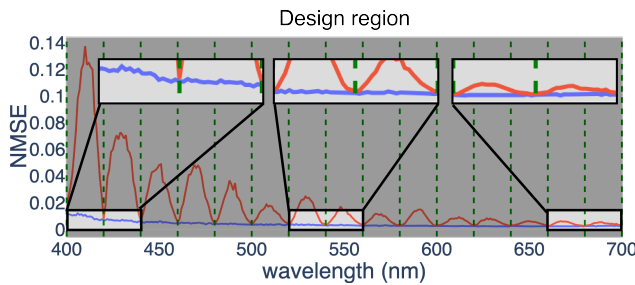


Figure A2: Comparison of design simulation region errors in the 400-700 nm wavelength range. The field prediction loss of WINO, particularly in the design region, exhibits a linear change as the wavelengths vary.

Nonlinearity of Subwavelength Photonic Structure Resonance

Mie scattering (Dorodnyy, Smajic, and Leuthold 2023; Nieto-Vesperinas 2020), a fundamental mechanism describing the interaction of electromagnetic waves with particles smaller

*These authors contributed equally.

†Corresponding author.

than the wavelength of light, is pivotal in understanding resonance phenomena in subwavelength photonic structures. The mathematical formulation of Mie scattering is expressed through an infinite series of spherical harmonics, where each term represents a different mode of scattering:

$$\sigma(\lambda, r) = \frac{2\pi}{k^2} \sum_{n=1}^{\infty} (2n+1) (|a_n|^2 + |b_n|^2)$$

where λ is the wavelength, r is the radius of the particle, $k = \frac{2\pi}{\lambda}$ is the wave number, and a_n, b_n are the scattering coefficients for electric and magnetic modes, respectively. The nonlinearity arises from the complex interaction between these modes, which can be highly sensitive to structural and material parameters, making accurate predictions difficult. Furthermore, high Q-factors are indicative of sharp resonance peaks and narrow bandwidths in the response of photonic structures, which implies that the system has a high selectivity in frequency response. While beneficial for many applications, high Q-factors also mean that the resonance is extremely sensitive to slight deviations in system parameters, such as changes in material properties or geometric alterations. This sensitivity leads to significant challenges in predicting the behavior of the system under slightly altered conditions:

$$Q = \frac{\omega_0}{\Delta\omega}$$

where ω_0 is the resonance frequency and $\Delta\omega$ is the bandwidth of the resonance.

At subwavelength scales, interactions between light and matter involve complex phenomena like electric and magnetic Mie resonances. Therefore, surrogate solvers trained at a single wavelength struggle to predict nonlinear resonances in regions with matter across broadband wavelengths. Our WINO model overcomes this challenge, accurately predicting resonances arising from structures.

We employ a wave prior based on the solution of the wave equation as the condition data ($\mathcal{W}_x = e^{j\frac{2\pi\sqrt{\epsilon_r}}{\lambda} x \mathbf{1}^T \Delta l_x}$ and $\mathcal{W}_z = e^{j\frac{2\pi\sqrt{\epsilon_r}}{\lambda} z \mathbf{1}^T \Delta l_z}$). However, when the relative permittivity, ϵ_r , reflects the materials used in the simulation, physically implausible features appear in the regions where the material is present (Figure A4). To resolve this, we set ϵ_r to 1, assuming the entire material is air. This approach allows us to obtain physically plausible features in free space.

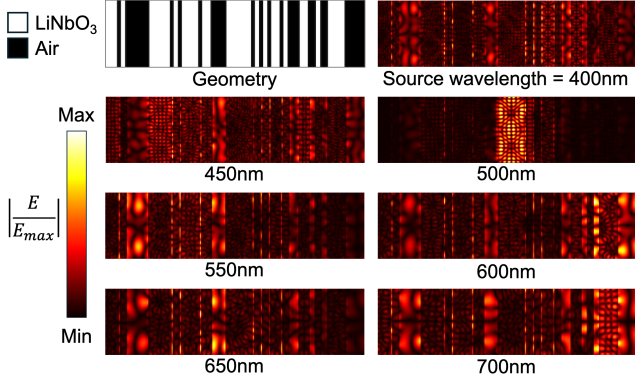


Figure A3: Using the FDTD simulation tool Meep, the E-field at the same time step is visualized for a design region composed of LiNbO_3 and Air. This visualization confirms that resonance occurs nonlinearly with respect to wavelength.

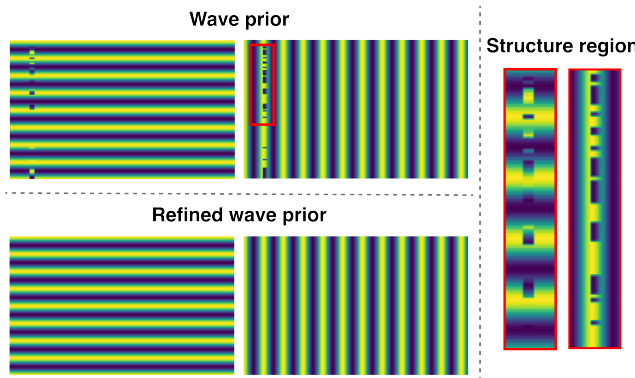


Figure A4: Visualization of (top left) wave prior that includes relative permittivity of materials, (right) physically implausible features of wave prior including relative permittivity of materials, and (bottom left) wave prior that excludes relative permittivity of materials.

Training Details

Our model training runs for 200 epochs with 16 batch size. The best model is selected based on the lowest loss in predicting previously unseen wavelengths during the training phase. We employ the GELU (Gaussian Error Linear Unit) activation function and the AdamW optimizer with the following parameters: a learning rate of 0.002, beta values of $(0.9, 0.000)$, epsilon set to 10^{-8} , and a weight decay factor of 0.0001. To dynamically adjust the learning rate, we utilize a cosine annealing learning rate scheduler with a minimum learning rate of 0.00001. Mode is set to $(50, 60)$. We leverage PyTorch, and the training process is conducted using a single RTX 6000 Ada.

Detailed Model Architectures

Unet We use a 4-level modern convolutional Unet architecture with an initial channel size of 16. Each level consists of two residual blocks with GELU activation function and

Group Normalization. We concatenate the refined wave prior with the input for the conditioning method.

FNO We set the number of Fourier layers and the number of channels in each Fourier layer to 5 and 32, respectively. The frequency modes for the z and x axes are set to $[32, 10]$. In addition, the lifting operator is a linear operator, and the projection operator is a 2-layer feed-forward network with GELU activation and a dimension of 128. We concatenate the refined wave prior with the input to inject condition information.

F-FNO We employ 12 Fourier layers, each consisting of 64 channels. The frequency modes for the z and x axes are set to $[50, 60]$. The lifting operator is a linear operator, and the final projection operator is a 2-layer feed-forward network with GELU activation function and a dimension of 256. To incorporate condition information, we concatenate the refined wave prior with the input.

NeurOLight We use 12 Fourier layers with 64 channels each. The frequency modes for the z and x axes are set to $[50, 60]$. The channel expansion factor for the convolutional modules in the NeurOLight layers is configured to be 2. To inject condition information, we concatenate the wave prior with the input. During training, we implement stochastic network depth with a rate of 0.1 to the residual NeurOLight layers to alleviate overfitting.

WINO We use 12 WINO layers with 64 channels each and specify the number of groups as 4. The frequency modes for the z and x axes are configured as $[50, 60]$. We implement a channel expansion scheme with a factor of 2 for the 2-layer feed-forward network in the WINO layers, inspired by [SegFormer, NeurOLight]. The lifting operator is linear, and the final projection operator is a 2-layer feed-forward network with GELU activation and a dimension of 256.

Additional Ablation Studies for Conditioning Methods

To verify the effectiveness of our conditioning method, we conduct an additional ablation study by applying the proposed conditioning method to other models and comparing it with other conditioning methods. “Unet-Bottleneck” maps the scalar wavelength value into a vector using a simple three-layers feed-forward network with GELU and then adds the induced condition vector to the input of the bottleneck in Unet. “Unet-AdaGN” reflects the wavelength condition in the model using Adaptive Group Normalization (AdaGN) (Dhariwal and Nichol 2021). The given wavelength value is transformed using sinusoidal embedding (Vaswani et al. 2017). Subsequently, a two-layer feed-forward network is used to project the embeddings into a higher-dimensional space of $4 \times$ hidden channels. The condition embeddings are incorporated into the Unet through AdaGN. “Unet, FNO, and F-FNO” refers to the method of concatenating the wave prior with the input data. Finally, “Ours” refers to our proposed conditioning method. According to Table A1, our method significantly improves the interpolation performance for unobserved wavelengths compared with the various conditioning methods of other models.

Model	Param (M)	Test loss		Design region test loss	
		Untrained	Trained	Untrained	Trained
Unet-Bottleneck	11.6371	0.11786	0.03303	0.059753	0.05574
Unet-AdaGN	11.779	0.09342	0.03548	0.047393	0.034908
Unet	11.5999	0.003332	0.001732	0.00619	0.003775
FNO	3.2868	0.0133	0.007719	0.028339	0.025067
FNO-Ours	3.2974	0.009966	0.008369	0.027739	0.028831
F-FNO	1.887	0.03309	0.02204	0.043035	0.037091
F-FNO-Ours	1.92	0.007606	0.006705	0.014702	0.014724

Table A1: Comparisons of field prediction and interpolation with various conditioning methods and models. Unet, FNO, and F-FNO refer to concatenating the wave prior with the input data. “Ours” represents our conditioning method.

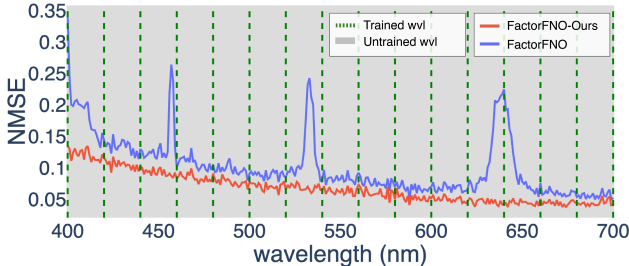


Figure A5: Field interpolation comparisons of F-FNO with simply concatenating conditioning and our conditioning method. Comparison of entire simulation region errors in the 400-700nm wavelength range.

When our conditioning method is applied to the FNO model, the field prediction performance for the wavelengths used during training is marginally reduced compared to when the method is not applied. However, there is a substantial performance improvement throughout the entire region for the unobserved wavelength data. In particular, the performance enhancement is dramatic in the case of F-FNO, which has conspicuously fewer parameters than Unet and FNO, factorizes the Fourier transforms over the problem dimensions, and is composed of many layers. Applying our conditioning method to F-FNO leads to a 77% increase in performance for unobserved wavelengths and a 67.6% increase for observed wavelength data across the entire simulation region compared with not using the conditioning method. In addition, in the design region, there is a 65.8% performance improvement for unobserved wavelengths and 60% improvement for observed wavelengths. We highlight that the error in the design region is consistent for both observed and unobserved wavelengths. Thus, we verify that our conditioning method substantially contributes to the interpolation capability.

Additional Experiments for the Weakened Precluded Assumption

We conducted additional experiments to evaluate the performance of our proposed method when the precluded assumption (that the field and condition data have high similarity) becomes weak. We set up the simulation with a more complex field using a material with higher relative permittivity

(lithium niobate, refractive index $n \approx 2.3$)¹.

FNO is inefficient in terms of the number of parameters. Despite having fewer layers and widths and lacking additional modules like fully connected layers, it has the highest number of parameters among the neural operators compared. As shown in Table A2², FNO struggles to learn complex optical properties even when our conditioning method is applied due to the limited learning capacity caused by the given problems. In contrast, F-FNO has sufficient capacity because of its superior parameter efficiency, which allows for many layers, widths, and additional MLPs. F-FNO demonstrates inferior performance despite its superior learning capacity if concatenating the wave prior with input data for conditioning. In particular, it exhibited peaks in the loss at specific wavelengths (Figure A5). On the other hand, applying our conditioning method to F-FNO significantly improves the field prediction performance and resolves the peak problem. This demonstrates that our method effectively helps to learn complex optical phenomena for a narrow range of wavelengths when sufficient learning capacity is available. While NeurOLight exhibits superior performance in field inference, it struggles to predict E-field across the broadband spectrum. However, WINO still demonstrates the best performance even when the precluded assumption becomes weak.

Weakening the Precluded Assumption in WINO

WINO element-wisely multiplies latent condition data at every layer. While the conditioning method serves as a powerful regularization means for interpolation on a wide range of conditions, it can have adverse effects when the precluded assumption is weakened due to more complex fields simulated from materials with high relative permittivity.

¹Permittivity is the square of the refractive index, denoted by n , which indicates how much light is refracted when it passes through a medium. Therefore, materials with higher permittivity have higher refractive indices. Consequently, when light passes through a material with high permittivity, it slows down more than in a material with lower permittivity, resulting in a more complex field pattern.

²The inference performance for untrained wavelengths often appears better than for trained wavelengths. This is because nonlinear optics phenomena (diffraction, resonance) caused by the high epsilon occur strongly, resulting in the loss exhibiting a slightly exponential change with respect to the wavelength. Consequently, if spectrum (condition) interpolation is successful, it can result in lower loss values for untrained wavelengths.

Model	Param (M)	Test loss		Design region test loss	
		Untrained	Trained	Untrained	Trained
Unet	11.5999	0.017035	0.018217	0.027433	0.028707
FNO	3.2868	0.120716	0.119495	0.334688	0.333512
FNO-Ours	3.2974	0.120637	0.121347	0.352237	0.352229
F-FNO	1.887	0.100673	0.111099	0.194343	0.196815
F-FNO-Ours	1.92	0.06785	0.070873	0.141015	0.143995
NeurOLight	1.65	0.016926	0.011881	0.0339	0.026632
WINO	0.426	0.007874	0.008075	0.01789	0.018281

Table A2: Comparisons of field prediction and interpolation with high relative permittivity.

Model	Param (M)	Test loss		Design region test loss	
		Untrained	Trained	Untrained	Trained
WINO	0.426	0.007874	0.008075	0.01789	0.018281
WINO ($l=1$)	0.417	0.007529	0.007858	0.017542	0.01809
WINO ($l=2$)	0.409	0.007451	0.007513	0.017448	0.017718
WINO ($l=3$)	0.401	0.008148	0.008231	0.019004	0.019232

Table A3: Field prediction and interpolation comparisons between injecting the condition into all but the last l WINO layers when relative permittivity is high.

To assess the effects of weakening the assumption in WINO, we conduct an ablation study, injecting information into layers except for the last l layers.

As shown in Table A3, injecting the condition into all but the last 1 and 2 WINO layers ($l = 1, 2$) reflects weakened assumption well and leads to performance improvement. However, injecting the condition into all but the final 3 WINO layers ($l = 3$) results in a decrease in both field inference performance and interpolation performance. This demonstrates the trade-off between the powerful regularization of our conditioning method and reflecting the weakened assumption.

References

Dhariwal, P.; and Nichol, A. 2021. Diffusion models beat gans on image synthesis. *Advances in neural information processing systems*, 34: 8780–8794.

Dorodnyy, A.; Smajic, J.; and Leuthold, J. 2023. Mie scattering for photonic devices. *Laser & Photonics Reviews*, 17(9): 2300055.

Nieto-Vesperinas, M. 2020. Fundamentals of Mie scattering. In *Dielectric Metamaterials*, 39–72. Elsevier.

Vaswani, A.; Shazeer, N.; Parmar, N.; Uszkoreit, J.; Jones, L.; Gomez, A. N.; Kaiser, Ł.; and Polosukhin, I. 2017. Attention is all you need. *Advances in neural information processing systems*, 30.